LAWRENCE
LIVERMORE
NATIONAL
LABORATORY

UCRL-JRNL-235660

2-D Coda and Direct Wave Attenuation Tomography in Northern Italy

P. Morasca, K. Mayeda, R. Gok, W. S. Phillips, L. Malagnini

October 18, 2007

Bulletin of The Seismological Society of America

Disclaimer

2-D Coda and Direct Wave Attenuation Tomography in Northern Italy

Paola Morasca[1], Kevin Mayeda [2], Rengin Gök[3], W.Scott Phillips [4], Luca Malagnini[5]

[1] University of Genova (Italy)
[2] Weston Geophysical Corporation (USA)
[3] Lawrence Livermore National Laboratory
[4] Los Alamos National Laboratory (USA)
[5] Istituto Nazionale di Geofisica e Vulcanologia (Italy)

Abstract

A 1-D coda method was proposed by *Mayeda et al.* (2003) in order to obtain stable seismic source moment-rate spectra using narrowband coda envelope measurements. That study took advantage of the averaging nature of coda waves to derive stable amplitude measurements taking into account all propagation, site, and *S*-to-coda transfer function effects. Recently this methodology was applied to micro earthquake data sets from three sub-regions of northern Italy (i.e., western Alps, northern Apennines and eastern Alps). Since the study regions were small, ranging between local-to-near-regional distances, the simple 1-D path assumptions used in the coda method worked very well. The lateral complexity of this region would suggest, however, that a 2-D path correction might provide even better results if the datasets were combined, especially when paths traverse larger distances and complicated regions. The structural heterogeneity of northern Italy makes the region ideal to test the extent to which coda variance can be reduced further by using a 2-D Q tomography technique. The approach we use has been developed by *Phillips et al.* (2005) and is an extension of previous amplitude ratio techniques to remove source effects from the inversion. The method requires some assumptions such as isotropic source radiation which is generally true for coda waves. Our results are compared against direct *S*-wave inversions for $1/Q$ and results from both share very similar attenuation features that coincide with known geologic structures. We compare our results with those derived from direct waves as well as some recent results from northern California obtained by *Mayeda et al.* (2005) which tested the same tomographic methodology applied in this study to invert for $1/Q$. We find that 2-D coda path corrections for this region significantly improve upon the 1-D corrections, in contrast to California where only a marginal improvement was observed. We attribute this difference to stronger lateral variations in Q for northern Italy relative to California.

Introduction

The goal of seismic monitoring, whether at local or regional distances, is to locate events and derive their source parameters accurately. At regional distances the problem is compounded because of very sparse station distribution with paths that often traverse complicated structures. The 1-D coda methodology introduced by *Mayeda et al.* (2003) for events along the Dead Sea fault demonstrate that coda waves allow for more stable results than using direct waves. Subsequent successful applications have been documented in California, Turkey, and Italy. In spite of lateral complexity, coda waves average over path and source variability. In Italy this approach was successfully applied to the western Alps (*Morasca et al.*, 2005a), eastern

Alps (*Malagnini et al.*, 2004), and northern Apennines (*Morasca et al.*, 2005b) where the simple 1-D radially symmetric path assumptions were sufficient to describe the regional scale complexity. However, the extension of this methodology to a larger and more laterally complex area including all three previously mentioned regions could require 2-D path corrections. For example, *Mayeda et al.* (2005) used northern California broadband data and found that though 2-D corrections improved over 1-D, the change was surprisingly small and 1-D corrections performed very well. The application of a tomographic approach to study the attenuation in Northern Italy will allows us to better understand the influence of the different structures on the average attenuation observed in the region. In fact, the presence of anomalies, such as the Ivrea body, is well known in this region (*Kissling* 1993; *Di Stefano et al.* 1999). It is also crucial to understand the detailed propagation effects for future accurate seismic hazard prediction.

Another purpose of this study is to improve the quality of the source spectra derived analyzing both coda and direct waves corrected using the 2-D attenuation models. This will allow for more accurate estimation of source parameters such as seismic moment (M_0) and radiated energy (E_R). Reliable estimates of such parameters make it possible to analyze the scaled energy ($? = E_R/M_0$) to understand the dynamics of the earthquake rupture process over a broad range of event sizes. In fact, the way earthquake radiated energy scales with event size is still debated in the scientific community (e.g., *Mayeda and Walter*, 1996, *Mayeda et al.*, 2007, *Morasca et al.* 2005a, *Ide and Beroza*, 2001; *Izutani and Kanamori*, 2001) because of the difficulties in energy estimation due to the strong influence of the attenuation and propagation effects, especially for small events (*Ide and Beroza*, 2001; *Izutani and Kanamori*, 2001).

To study the 2-D attenuation effects some authors (e.g., *Campillo et al.*, 1993; *Phillips et al.*, 2001) have estimated the attenuation by analyzing different phase amplitude ratios in order to remove source effects. There are also techniques that allow for the elimination of both source and site effects using two-station spectral ratios (e.g., *Chun et al.*, 1987; *Fan and Lay*, 2002; *Fan and Lay*, 2003; *Shih et al.*, 1994), with the limit that a collinear alignment of event and receiver pairs is required.

Another amplitude ratio tomography method has been developed by *Phillips et al.* (2005), which provides for high resolution Q images with the advantage of reducing the number of terms in the inversion. By assuming that the distance-dependence for coda envelope and direct amplitudes can be described using the same form (i.e., Q and geometrical spreading), *Mayeda et al.* (2005) successfully tested this method using early coda measured in northern California. Several studies (*Wagner*, 1997;1998) showed that the early coda has very similar back-azimuths to the direct arrival and it is only the late coda which seems to be truly random. This means that a tomographic approach is appropriate when using early coda.

For this study we apply the same amplitude ratio tomography method to obtain 2-D attenuation corrections in northern Italy for both direct and early coda waves. We then compare the performance with the 1-D approach using the same data set. We expect that the 2-D attenuation corrections will improve the stability of the final corrected source spectra, taking into account the complexity of the region. In fact, northern Italy is characterized by different geological structures such as the sedimentary basin of the Po valley which is bounded by the northern Apennines to the south and by the Alpine chain to the north (figure1). As suggested by many authors (e.g., *Castro et al.*, 1999; *Mele et al.*, 1997; *Carletti and Gasperini*, 2003) the Po valley is generally characterized by efficient S-wave propagation with respect to the western

Alps and the northern Apennines. In contrast, high attenuation is observed in the northern Apennines due to the presence of high heat flow (*Ponziani et al.,* 1995).

Data

We used more than 400 earthqua kes with magnitude larger than M_L ~ 3.0 that were mainly recorded by 19 three -component stations of the RSNI network (Regional Seismic network of Northwestern Italy, Genova). In addition, we supplemented this dataset to gain better path coverage by using waveforms from the RéNaSS (The French National Network of Seismic Survey, Strasbourg) , 4 from OGS network (Istituto Nazionale di Oceanografia e di Geofisica Sperimentale, Trieste, Italy) and 2 from GRSN network (Germany). Figure 2 shows a map of stations and events used in this study. For specific details of the data, we refer the reader to previous local coda studies in this region (e.g., *Morasca et al.*, 2005a; *Malagnini et al.*, 2004; *Morasca et al.*, 2005b). In general, inversions for both wave types used essentially the same number of data, however, in some cases direct *S*-waves were clipped and discarded, whereas the coda was perfectly useable. In other cases, the coda's signal-to-noise ratio was too low but the direct *S*-wave was useable.

Method

Amplitude measurements

For each of the following 10 frequency bands: 0.3 -0.5, 0.5-0.7, 0.7-1.0, 1.0-1.5, 1.5-2.0, 2.0-3.0, 3.0-4.0, 4.0-6.0, 8.0 -10.0, 10.0-15.0-Hz, we measure direct *S*-waves and early coda envelope amplitudes for our data set. In general, coda window lengths were limited to roughly 60 seconds from the direct *S*-wave for frequencies 1.0-Hz and larger and roughly 100 seconds for frequencies below 1-Hz. Coda envelopes are formed from each horizontal component and then averaged for additional stability. The smoothed version of each coda envelope is empirically described following *Mayeda et al*. (2003) that used a simple functional form:

$$A_c(f_i,t,r) = W_o(f_i)\cdot S(f_i)\cdot T(f_i)\cdot P(r,f_i)\cdot H\left(t-\frac{r}{v(r,f_i)}\right)\cdot\left(t-\frac{r}{v(r,f_i)}\right)^{-q(r,f_i)}\cdot exp\left[b(r,f_i)\cdot\left(t-\frac{r}{v(r,f_i)}\right)\right] \quad (1)$$

where $W_o(f_i)$ is the *S*-wave source amplitude, $S(f_i)$ is the site response, $T(f_i)$ is the *S*-to-coda transfer function resulting from scattering conversion, $P(r,f_i)$ includes the effects of geometrical spreading and attenuation (both scattering and absorption), *H* is the Heaviside step function, $v(r,f_i)$ is the peak velocity of the *S*-wave arrival, $g(r,f_i)$ and $b(r,f_i)$ control the shape of the early coda immediately following the S waves and *t* is the time in seconds from the origin time. The early coda amplitude measurements (A_c) are obtained by fitting the observed envelopes. The raw a mplitudes are then path corrected using 1-D and 2-D attenuation formulations described below. We refer the reader to *Mayeda et al.* (2005) for specific details of the method.

1-D Path corrections

The coda path correction outlined in *Mayeda et al.* (2003) is empirically based and was meant to mimic observed local and near regional coda observations. The main observations are that local coda are homogeneously distributed in space and time, in sharp contrast to direct *S*-waves which decay with increasing distance (e.g., see Figure 1 of *Mayeda et al.*, 2005). However, we are finding that at local distances, the coda shape parameter in Equation 1 is strongly distance dependent, perhaps a result from transitioning from local *S*-wave coda to regional L_g-coda. Figure 3 shows example synthetic envelopes for a unit source at a range of distances. Though the direct arrivals are the same level, the coda amplitudes clearly change with distance and results in a trade-off between the coda envelope shape parameter, $b(r,f)$ and the attenuation parameter, $P(r,f)$. Therefore, if the same source were measured at a range of distances, we would not get the same coda amplitude, a result from an artefact of the calibration process. To remedy this calibration bias at short distances, we needed another free parameter to correct our synthetic envelopes to better match observations. A functional form that could empirically correct for this bias stems from the local and regional geometrical spreading formulation of *Street et al.* (1975). Our new 1-D geometrical spreading function is coined the name, *Extended Street & Herrmann*, or ESH. Instead of one critical distance, where the spreading value is changed, we use a distance range where the transition changes smoothly. We note again that this is not physical, but merely a necessity due to the calibration process. The new spreading function is the product of individual transition terms as described below for three separate distance ranges of x:

$$f(x) = x^{-a_1} \qquad x < X_1 \qquad (2a)$$

$$f(x) = (X^{-a_1})(x/X_1)^{-(a_1+\Delta a(x)/2)}$$
$$\Delta a(x) = \log(x/X_1)(a_2 - a_1)/\log(X_2/X_1) \qquad X_1 < x < X_2 \qquad (2b)$$

$$f(x) = (X^{-a_1})(X_2/X_1)^{-(a_1+\Delta a(x)/2)}(x/X_2)^{-a_2} \qquad x > X_2 \qquad (2c)$$
$$\Delta a(x) = (a_2 - a_1)$$

where $X_1 = X_0/F$ and $X_2 = X_0 * F$ where X_0 is the critical distance and F is the transition factor (= 1). $\Delta a(x)$ is the interpolated increase in spreading relative to a_1. We compared performance between the original *Mayeda et al.* (2003) path formulation and the modified version above and found up to 30% improvement in data standard deviations, especially at higher frequencies.

Next, assuming that the distance-dependence has the same form (i.e., Q and geometrical spreading) for both coda and direct amplitudes (*Mayeda et al.*, 2005), we correct for the geometrical spreading and estimate the Q effect.

A similar approach is used for the direct waves to obtain the best *S*-wave quality factor (Q_S) that minimizes the scatter between all station pairs (see *Mayeda et al.* 2003). Following *Yang's* (2002) synthetic results, we assume a $1/r$ geometrical spreading, and used the following relation:

$$A(r,f) = A_0 S(f) \frac{1}{r} e^{-\left|\frac{\pi f}{bQ_b}\right|} \qquad (3)$$

where A_0 is the source, S is the site effect, b is shear-wave velocity. We tested more complicated geometrical spreading functions from previous ground-motion scaling studies from the same regions (e.g., *Morasca et al.*, 2006; *Malagnini et al.*, 2002) and found that there was no difference in our final results since the choice of Q trades-off with the spreading function.

2-D Path corrections

The attenuation tomography technique (*Phillips et al.*, 2005) is based on amplitude ratios taken between stations that recorded the same event. This eliminates the source term from the inversion but one must assume an isotropic source radiation. Coda amplitudes derived using *Mayeda et al.* (2003) coda calibration procedure, and direct waves measurements are independently used as input to the inversion. Using short coda, we can describe path effects in the same way of the direct waves rather than an ellipsoidal area so that a tomography approach is appropriate.
Again, we use the 1-D ESH path corrections on the coda amplitudes, then invert for the spatially varying Q.

The following amplitude ratio formulation was applied:

$$A_{ij} - \langle A_{ij} \rangle_j = S_i - \langle S_j \rangle_j + (P_k\, dx_{ijk}\, a_k - \langle P_k\, dx_{ijk} \alpha_k \rangle_j) \log_{10}(e) \qquad (4)$$

Where A is $\log_{10}$ spreading corrected amplitude, i, j, k indices are site, source and path discretization respectively, S is the $\log_{10}$ site terms, and dx are the path lengths through a discretized region of the Earth, a is the discretized attenuation coefficient ($\alpha_k = \omega / 2Q_k c$), and P_k are the raypath sums. The ratio is taken between the single value and the average for the same event j, consequently the source ratio is zero. We obtain a linear system of equations and solve using sparse matrix methods. Smoothing constraints are applied to the attenuation model to avoid artefacts due to noise, and the site terms sum is assumed to be zero. We obtained a tomography image for each frequency band in a range between 0.3 and 15-Hz for coda and direct waves separately.

At this point we have four different cases that need to be analyzed:

i) direct waves amplitudes path corrected using 1-D attenuation parameters;
ii) coda waves amplitudes path corrected using 1-D attenuation parameters;
iii) direct waves amplitudes path corrected using 2-D attenuation parameters;
iv) coda waves amplitudes path corrected using 2-D attenuation parameters.

For each of these four sets of path-corrected amplitudes, source spectra are computed following the approach used by *Mayeda et al.* (2003).

Attenuation tomography results

For each frequency band in the range of 0.3 – 15-Hz we imaged quality factor variations with respect to an average computed over the region. Figure 4 shows Q tomography results for all the frequency bands for the direct waves while figure 5 displays the results obtained for the coda waves analysis. In all cases we used pixel

dimensions of 0.1 degrees. Results are presented as difference in % from the average Q (green) for each frequency. The average Q ($<Q>$) value is reported in the bottom of each plot and increases with increasing frequency for both wave types.

We observe that both wave types exhibit low attenuation in the southern part of the western Alps that coincides with the area characterized by the massifs. This anomaly is observable starting from 0.7 - 1.0 Hz for the direct waves and from 1.5 - 2.0 Hz for coda waves. *Eva et al.* (1991) obtained similar results in their study analyzing coda Q variations focusing on this restricted area. In addition, a large low Q area to the north is observed for both direct and coda analysis. In this case, the anomaly is observable at all frequencies, but with slightly different lateral extent. Except for very low and high frequencies, the anomalous area seems to narrow around the Ivrea body, known as a shallow slice of mantle (*Kissling* 1993; *Di Stefano et al.* 1999). The presence of this body seems to have important effects such as the production of a positive Bouguer anomaly (*Vernant et al.* 2002). Moreover, in the same zone an extinction of L_g waves was observed by *Campillo et al.* (1993) over a wide frequency range. Their results confirm our findings since the authors explain this attenuation effect as a result of strong lateral heterogeneity of the surface geology which is characterized by interwoven mantle and crustal rocks. They interpret the wide range of frequency in which the extinction is observable as due to variable scale-length heterogeneities within the area.

Figures 4 and 5 also show a high Q zone in correspondence with the Po plain, extending to the very northern part of the Apennines, close to Parma (see figure 1). As for the high Q zone of the northernmost part of the Apennines, an interpretation is not simple given the complex geological setting and geometric crustal relationships. In fact, the northern Apennines' front is buried under the Po plain sediments and the Po plain is the foreland basin of both the Alps and Apennines (*Doglioni*, 1993). This complexity might be the origin of strong lateral heterogeneity in the crust where we observe a high attenuation anomaly related to this buried front. It is clear that the anomaly we observe in this area is not a result of artefacts correlated to the adopted methodology or to the data and station distribution since other studies show an anomalous propagation of waves within this region. In fact, *Ciaccio and Chiarabba* (2002) observed a shallow, high velocity anomaly in the same area and interpreted that as an effect of heterogeneity due to uplifted Mesozoic carbonaceous rocks. Moreover, a recent study of *Margheriti et al.* (2006) highlight a seismic anisotropy in this area finding a shear wave splitting effect that the authors relate to the presence of fluid-saturated micro-cracks aligned or opened by the prevailing stress field.

Tests with synthetic data have been conducted to reveal inherent limitations in resolution and possible artifacts due to event-station geometry and chosen parameterization. For each frequency band we performed checkerboard tests to verify what could and could not be resolved. In all cases the results look very similar each other except at the lowest bands for which we needed to use a larger grid size. Figure 6 shows example results for a representative range of frequency bands. The low and high attenuation input cell values vary as a function of frequency, in accordance to what we observe in the real data. We recognize however that high Q regions will not be well resolved due to smoothing of adjacent low Q regions. The accurate recovery of high Q is known to be an issue because of smoothing constraints on $1/Q$, but our derived model still fits the data well, and path corrections can be predicted from the model equally well. Therefore, this does not affect our overall interstation amplitude performance. In other words our low Q results are very close to the input value but the high Q pixels in our checkerboard are roughly a factor of 2 to 3

lower than actual. This is a very common phenomenon that happens due spatial smoothing, thus making it difficult to resolve high Q regions (*Xie*, 2005).

Performance comparison

For both direct and coda waves we corrected the raw amplitudes using the 1-D and 2-D frequency-dependent attenuation parameters. Then for the same events we compared distance-corrected amplitude scatter for the same station pairs to evaluate the relative performance of each method. Figure 7 shows, for each method, the average standard deviation among 37 station pairs for each frequency band.

As expected, using a 2-D path correction results in lower standard deviations with respect to using 1-D path corrections for both direct and coda waves. However, when we compare 2-D direct wave standard deviation with 1-D coda waves results, we observe that even if we use a simple 1-D model, coda measurements are more stable. The best performance is obtained for 2-D path-corrected coda amplitudes. We note that in general, our results are very similar to those from northern California (*Mayeda et al*, 2005). However, we find that there is a larger improvement between 1-D coda and 2-D coda for our current study region. We hypothesize that this is due to stronger lateral variations in Q relative to northern California. From a seismic monitoring standpoint, this is important because it shows that some regions can benefit significantly from 2-D coda path calibrations.

Source Spectra

For all four cases the path-corrected amplitudes are used to compute source spectra. Further frequency-dependent site and S-to-coda transfer function corrections were derived using the procedure outlined by *Mayeda et al.* (2003). Likewise for the direct wave amplitudes, we applied similar corrections to remove site effects and derive absolute source spectra. An example of the November 24th, 2002, M_W 5.1 event is plotted in figure 8, where grey and black curves are the station and average source spectra, respectively. The scatter observed for the different cases reflects the results presented in figure 7. As expected, source spectra derived from coda measurements are much less scattered than those computed from the direct waves, and the most stable results are obtained for coda measurements when we use the 2-D attenuation corrections.

Discussion and Conclusions

For the same data set and stations we estimated the attenuation effects for both coda and direct S waves using a new 2-D tomography approach (*Phillips at al*, 2005) as well as performed a comparison with the 1-D method outlined by *Mayeda et al.* (2003). For the coda wave analysis we focused on the early coda since, as many studies demonstrated (e.g., *Wagner*, 1997 1998) the late coda consists of multiple scattered energy that samples a larger volume of the propagation medium, more so than the early coda and the direct waves. This means that the early coda path effects could be roughly approximated to the direct waves and used in a traditional direct-wave tomographic approach.

Attenuation tomography revealed lateral complexity for northern Italy which comprises the Alps-Apennines junction zone and the foredeep basin (Po plain) of both

chains. Our results consistently show the same trend for different frequency bands and for both coda and direct waves, though lateral coda attenuation is smoother, especially for high and low frequencies. This effect is expected because of the averaging nature of coda waves and is consistent with observations by *Mayeda et al.* (2005) for northern California.

A low attenuation area is observed in the southern part of the Western Alps, in agreement with results by *Eva et al.* (1991) who focused their coda Q study in this small zone of western Alps characterized by the presence of crystalline massifs. To the north of this zone, in the western Alps, a large low Q anomaly is observed in correspondence with the Ivrea body, in good agreement with an L_g extinction observed in the same area by *Campillo et al.* (1993). *Campillo et al.* (1993) suggest that the blockage of *Lg* across the western Alps as being due to the effect of low Q from the presence of strong heterogeneity of the crust. The large range of frequency in which the anomaly is observed indicates a variable scale-length of the heterogeneity. Our results also show high Q under the Po Plain, the largest alluvial basin of Northern Italy. This region has a complex geological and structural setting since the thrust fronts of the northern Apennine are buried by variable thickness, Quaternary alluvium (*Pieri and Groppi*, 1998) that might cause the anomalous propagation. The behaviour within this region is confirmed by other studies indicating the presence of velocity (*Ciaccio and Chiarabba*, 2002) and seismic (*Margeriti et al.* 2006) anomalies.

The attenuation results obtained from the tomography have been used to derive source spectra. We compared direct and coda waves using 1-D and 2-D attenuation corrections, and demonstrated that the 2-D method provides more stable results than the 1-D approach for the same phase. However, when we compare direct and coda waves, we notice that the simple 1-D attenuation corrections applied to coda measurements are significantly better than direct S-waves corrected for 2-D attenuation. The same conclusion was reached by *Mayeda et al.* (2005) for northern California. Since the study area is relatively small and limited in data, we plan to add more events and stations from other networks to enlarge the study area to better understand the relationship between attenuation and geological structures for the broader region.

Acknowledgements

The authors wish to thank Prof. C. Eva and the RSNI network staff for the careful network management and data collection that made this work possible. We wish to thank the OGS, Trieste, for kindly providing some data from their seismic network. The helpful suggestions of two anonymous reviewers and of the editor Hiroshi Kawase helped us to improve this manuscript. K. Mayeda was supported under Weston Geophysical subcontract No. GC19762NGD and AFRL contract No. FA8718-07-C-0010. This work performed under the auspices of the U.S. DOE by Lawrence Livermore National Laboratory under Contract DE-AC52-07NA27344.

References

Campillo, M., Feignier, B., Bouchon, M. Ad N. Béthoux (1993). Attenuation of Crustal Waves Across the Alpine Range . *J. Geoph. Res.* 98, B2, 1987-1996.

Carminati, E., Doglioni, C and D. Scrocca (2004). Alps vs Apennines. *Special Volume of the Italian Geological Society for the IGC 32 Florence-2004.*

Carletti, F. and P. Gasperini (2003). Lateral variations of seismic intensity attenuation in Italy. Geophys. J. Int. 155, 839 -856.

Castro, R.R., M. Mucciarelli, G. Monachesi , F. Pacor and R. Berardi (1999). A review of nonparametric attenuation functions c omputed for different regions of Italy. Ann. Geofisica, 42, 735-748.

Chun, K.-Y., G. F. West, R. J. Kokoski, and C. Samson (1987), A novel technique for measuring Lg attenuation: Results from eastern Canada between 1 to 10 Hz, *Bull. Seismol. Soc. Am.,* 77, 398– 419.

Ciaccio, M. G. and C. Chiarabba (2002). Tomographyc models and seismotectonics of the Reggio Emilia region, Italy. *Tectonophysics* 344, 261-276.

Di Stefano, R., Chiarabba, C., Lucente, F., and A. Amato (1999), Crustal and uppermost mantle struct ure in Italy from the inversion of P-wave arrival times: geodynamic implications . *Geophys. J. Int.* **139**, 483-498.

Doglioni, C. (1993). Some remarks on the origin of foredeeps. *Tectonophysics* **228**, 1– 20

Eva, C., Cattaneo, M., Augliera, P., and Pasta, M., 19 91, Regional coda Q variations in the western Alps (northern Italy). *Phys. Earth Planet. Inter.* **67**, 76-86.

Fan, G.-W., and T. Lay (2002). Characteristics of *Lg* attenuation in the Tibetan Plateau, *J. Geophys. Res.* **107** no. 10, 2256, *doi* 10.1029/ 2001JB00080 4.

Fan, G., and T. Lay (2003), Strong Lg wave attenuation in the Northern and Eastern Tibetan Plateau measured by a two -station/two-event stacking method, *Geophys. Res. Lett.,* 30(10), 1530, doi:10.1029/2002GL016211.

Ide, S. and G. C.,Beroza (2001), Does apparent stress vary with earthquake size? *Geophys. Res. Lett.,* **28**,3349-3352.

Izutani, Y. and H., Kanamori (2001), Scale -dependance of seismic energy-to-moment ratio for strike-slip earthquakes in Japan. *Geophys. Res. Lett.,* **28**, 4007-4010.

Kissling, E., (1993). Deep structure of the Alps —what do we really know? *Phys. Earth planet. Inter.,* **79**, 87-112.

Malagnini, L., A. Akinci, R. G. Herrmann, N. A. Pino, L. Scognamiglio (2002). Characteristics of the ground motion in Friuli (Northeastern Italy), Bull. Se ism. Soc. Am. v. 94; no. 4; p. 1343 -1352.

Malagnini, L., Mayeda, K., Akinci, A. and P. Bragato (2004). Estimatine absolute site effects. Bull. Seism. Soc. Am. v. 94; no. 4; p. 1343 -1352.

Margheriti, L., Ferulano, M. F., Di Bona, M. (2006). Seismic anisot ropy and its relation with crustal structure and stress field in the Reggio Emilia Region (Northern Italy). *Geophys. J. Int* **167**, 1035-1043.

Mayeda, K. and W. R.,Walter (1996). Moment, energy,stress drop, and source spectra of western United States earthquakes from regional coda envelopes. *J. Geophys. Res.,* 101, 11.195-11.208.

Mayeda, K., A. Hofstetter, J. L., O'Boyle, and W. R. Walter (2003), Stable and Transportable Regional Magnitudes Based on Coda -Derived Moment-Rate Spectra. *Bull. Seismol. Soc. Am.* 93: 224–239.

Mayeda, K., Malagnini, L., Phillips, W. S., Walter, W. R. and D., Dreger (2005). 2-D or not 2 -D, that is the question: A northern California test. *Geophys. Res. Lett.,* 32, L12301, doi:10.1029/2005GL022882.

Mayeda, K., L. Malagnini, W.R. Walte r, A new spectral ratio method using narrow band coda envelopes: Evidence for non -self-similarity in the Hector Mine sequence, *Geophys. Res. Lett.*, doi:10.1029/2007GL030041, 2007.

Mele, G., Rovelli, A., Seber, D. and M., Barazangi (1997) Shear wave attenu ation in the lithosphere beneath Italy and surrounding regions: Tectonic implications. *J. Geophys. Res.* 102 no. B6, 11,863-11,875.

Morasca, P., Mayeda K., Malagnini, L. and W. R Walter (2005a). Coda Derived Source Spectra, Moment Magnitudes, and Energy -Moment Scaling in the Western Alps. *Geoph. J. Int.* **160** (1), 263-275.

Morasca, P., Mayeda, K., Gök, R., Malagnini, L., Eva C. (2005b). A break in self -similarity in the Lunigiana -Garfagnana region (Northern Apennines). *Geoph. Res. Lett.* Vol. 32, No. 22, L22301 10.1029/ 2005GL024443

Morasca, P., Malagnini, L., Akinci, A., Spallarossa D. (200 6). Ground Motion Scaling in the Western Alps. *Journal of Seismology (in press).*

Phillips, W. S., Hartse, H. E., S. R., Taylor, A. A. Velasco and G. E. Randall (2001). Application of regional phase amplitude tomography to seismic verification. *Pure Appl. Geophys*., 158, 1189-1206.

Phillips, W. S., Hartse, H. E. and J. T. Rutledge (2005), Amplitude ratio tomography for regional phase Q. Geophys. Res. Lett. Vol. 32, no 21, L 21301,doi: 10.1029/2005GL023870.

Pieri, M., and G. Groppi, (1998). Subsurface geological structure of the Po Plain, Italy. *AGIP-CNR Progetto Finalizzato Geodinamica,* pub. 414, Roma.

Ponziani, F., De Franco, R., Minelli, G., Biella, G., Federico, C., Pial li, G., (1995). Crustal shortening and duplic ation of the Moho in the Northern Apennines: a view from seismic reflection data, *Tectonophysics*, **252**, 391 418.

Shih, X. R., K.-Y. Chun, and T. Zhu (1994), Attenuation of 1-6s Lg Waves in Eurasia. *Geophys. Res.,* Vol. 99, No. B12, 23859-23874.

Street, R. L., R. Herrmann, and O. Nuttli (1975). Spectral characteristics of the Lg wave generated by central United States earthquakes*, Geophys. J. R. Astron. Soc*. **41**, 51-63.

Vernant, P., Masson, F., Bayer, R., and A. Paul (2002). Sequential inversion of local earthquake traveltimes and gravity anomaly – the example of the Western Alps. *Geophys. J. Int.* **150**, 79-90.

Xie, J. (2005). On the Inadequacy of Stochastic Modeling of Regional Lg Wave Spectra. Eos Trans. AGU, 86(52), Fall Meet. Suppl., Abstract S43C-05.

Yang, X. (2002). "A numerical investigation of Lg geometrical spreading," *Bull. Seism. Soc. Am.,* Vol. 92, 3067-3079.

Wagner G. S. (1997), Regional wave propagation in southern California and Nevada: Observations from a three-component seismic array. *J. Geophys. Res.*, 102(B4), 8285–8312.

Wagner G.S. (1998), Local wave propagation near the San Jacinto fault zone, southern California: Observations from a three-component seismic array. *Bull. Seismol. Soc. Am., 103*, 7231-7246.

Figures captions

Figure 1 – Simplified tectonic map of Northern Italy derived by *Carminati et al.* (2004). 1) foreland areas; 2) foredeep deposits; 3) domains characterised by a compressional tectonic regime in the Apennines; 4) thrust belt units accreted during the Alpine orogenesis in the Alps and in Corsica; 5) areas affected by extensional tectonics; 6) outcrops of crystalline basement; 7) regions characterised by oceanic crust; 8) Apennines water divide; 9) thrusts; 10) faults.

Figure 2. Data and stations used in this study. Triangles indicate RSNI stations, squares OGS stations, circles GRSN stations and the diamond indicates the RéNaSS station.

Figure 3. Synthetic coda envelopes for the same unit source at 50 km intervals. Notice that the direct arrivals are the same level, but the coda envelope levels change with distance due to $b(r,f)$ in Equation 1 changing rapidly in the first ~100 km. This bias in envelope amplitude level, however, is accounted for in our new path correction formulation.

Figure 4 - The 2-D inversion results for direct waves for all analyzed frequency bands. The value of $< Q >$ at the bottom of each image is the average quality factor for the resolved area (the colored portion of each map) for each frequency. The col or scale

indicates the variation in percentage with respect to $<Q>$. White triangles represent the stations while black circles are the events used for each inversion.

Figure 5 - Q tomography results for coda waves at all frequency bands. Each image shows the variation of Q in percentage with respect to the average value reported at the bottom of each image ($<Q>$). The colored portion of each map delineated the region where we have good resolution. White triangles represent the stations while black circles are the events used for each inversion.

Figure 6 - Result of checkerboard tests for the frequency bands 0.3-0.5 Hz where we have used a cell size of 1.0 X 1.0 degrees; 1.5-2.0 Hz and 10. 0-15.0 Hz using cells of 0.50 X 0.50 degrees. The input model is shown in the top corner of each image as a reference. The low and high attenuation input values vary as a function of frequency, in accordance to what we observe in the real data. The polygon delineates the region where we have a good resolution generally for all frequency bands.

Figure 7 –Averaged inter-station standard deviation using 37 station pairs as a function of frequency. The 1-D and 2-D methodologies applied to direct and coda waves have been compared and the results show that the tomographic method (2-D) applied on coda waves gives the best results with the lowest standard deviations.

Figure 8 – Example of moment-rate spectra obtained for the 2002, November 24th, M_W=5.1 event. Gray curves are the individual station spectra while black curves represent the averages. Stations are situated at a variety of azimuths and distances. As expected, direct waves results are more scattered then coda waves for both 1-D and 2-D methods, consistent with the finding shown in Figure 7.

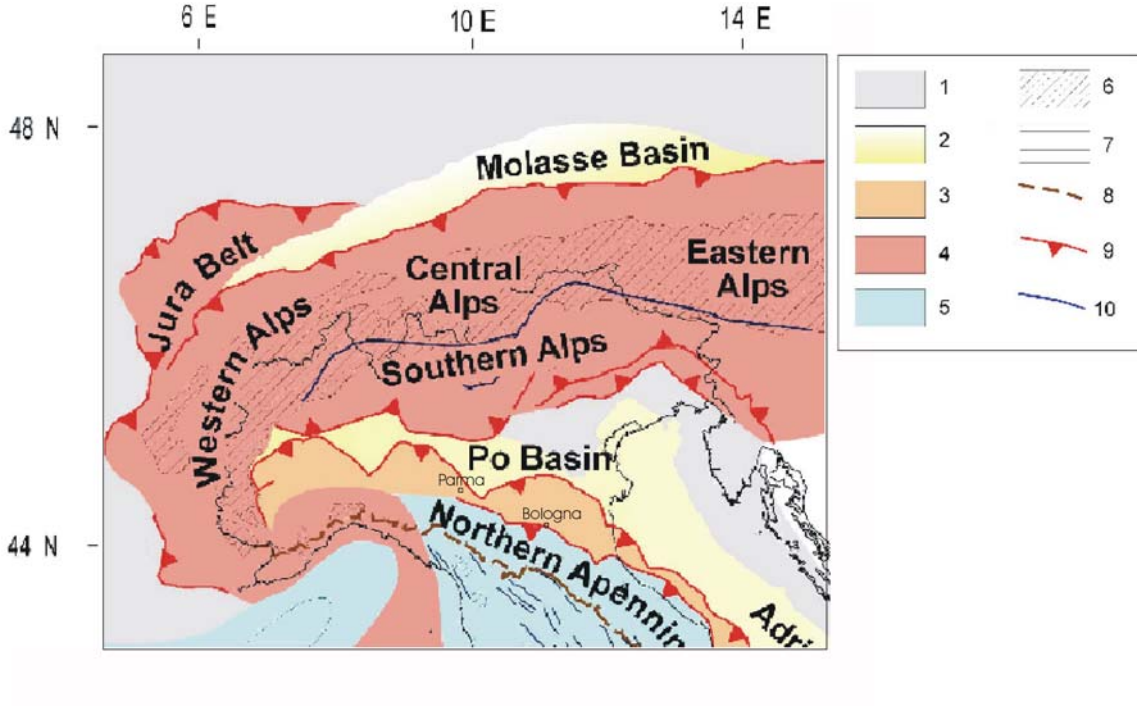

Figure 1 – Simplified tectonic map of Northern Italy derived by Carminati et al. (2004). 1) foreland areas; 2) foredeep deposits; 3) domains characterised by a compressional tectonic regime in the Apennines; 4) thrust belt units accreted during the Alpine orogenesis in the Alps and in Corsica; 5) areas affected by extensional tectonics; 6) outcrops of crystalline basement; 7) regions characterised by oceanic crust; 8) Apennines water divide; 9) thrusts; 10) faults.

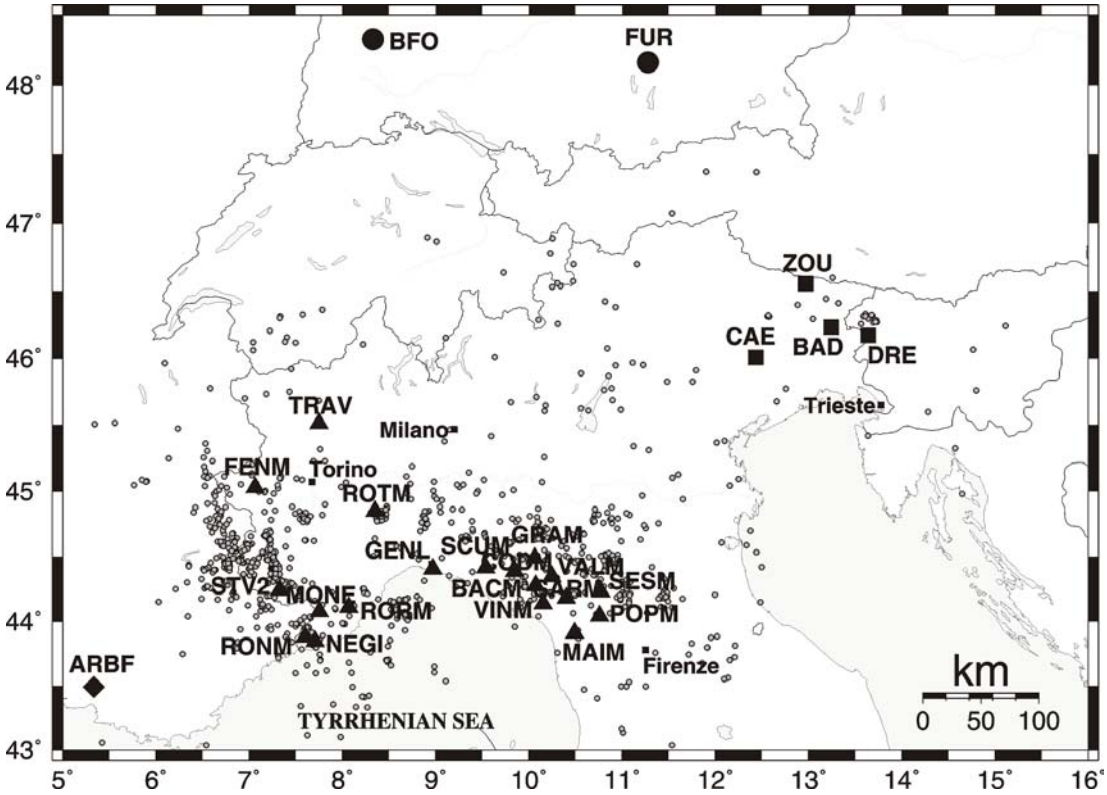

Figure 2. Data and stations used in this study. Triangles indicate RSNI stations, squares OGS stations, circles GRSN stations and the rhombus indicates the RéNaSS station.

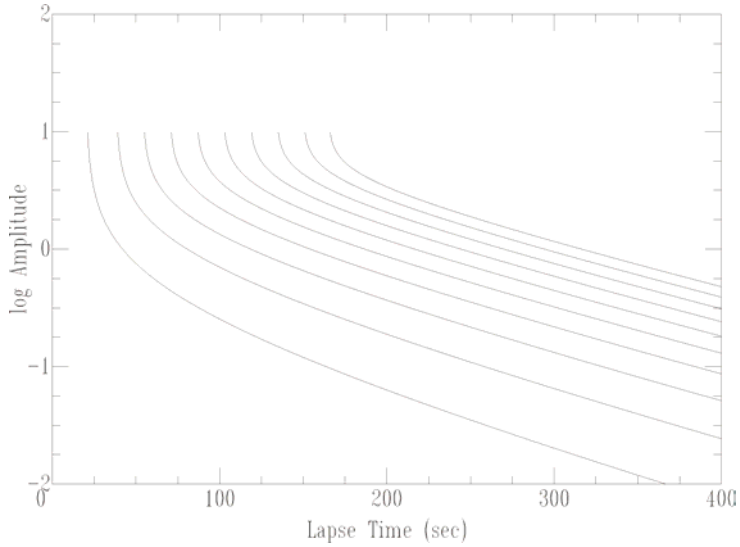

Figure 3. Synthetic coda envelopes for the same unit source at 50 km intervals. Notice that the direct arrivals are the same level, but the coda envelope levels change with distance due to $b(r,f)$ in Equation 1 changing rapidly in the first ~100 km.

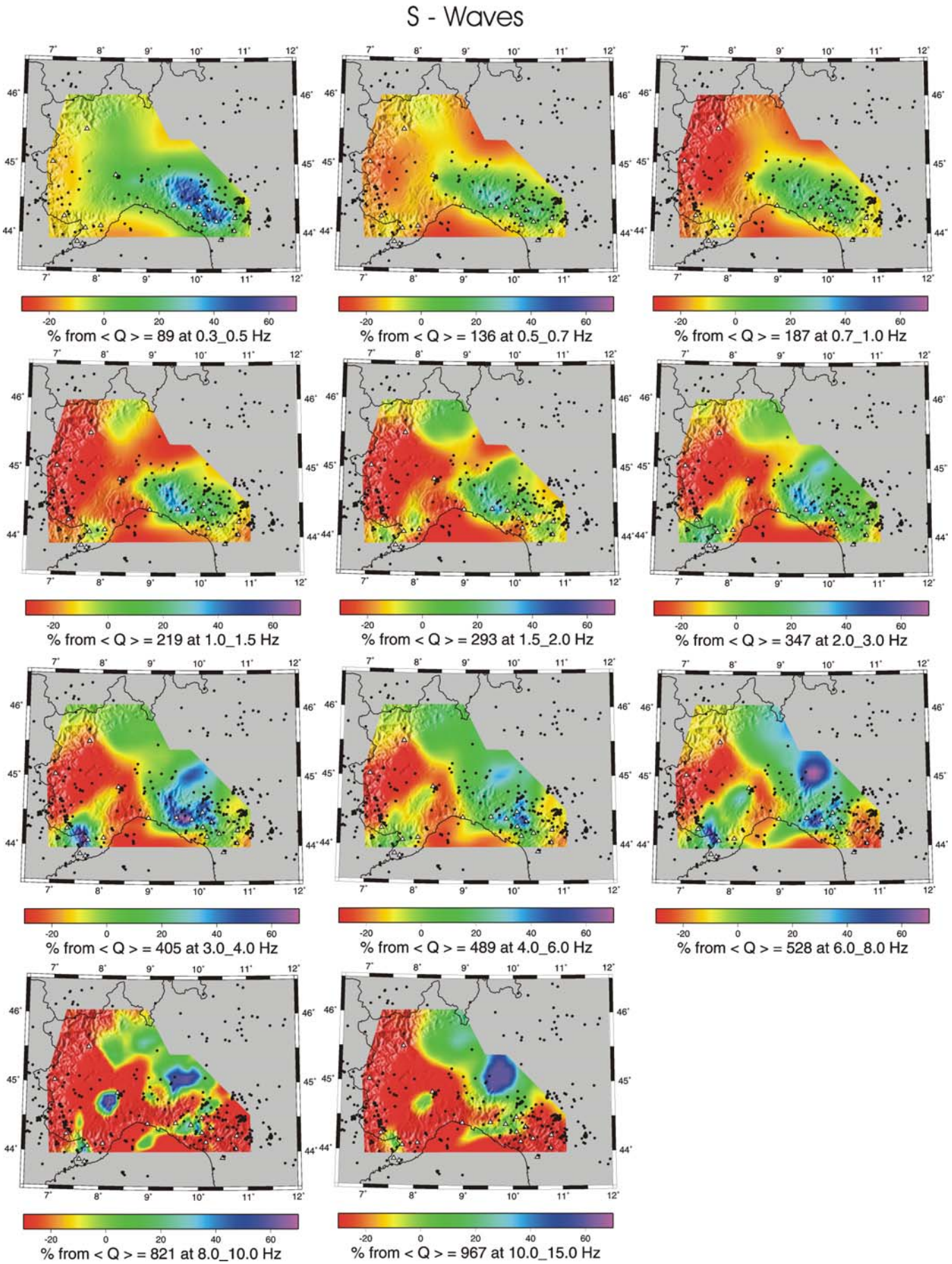

Figure 4 - The 2-D inversion results for direct waves for all analyzed frequency bands. The value of <Q> at the bottom of each image is the average quality factor for the resolved area (the colored portion of each map) at the considered frequency. The color scale indicates the variation in percentage with respect to <Q>. White triangles represent the stations while black circles are the events used for each inversion.

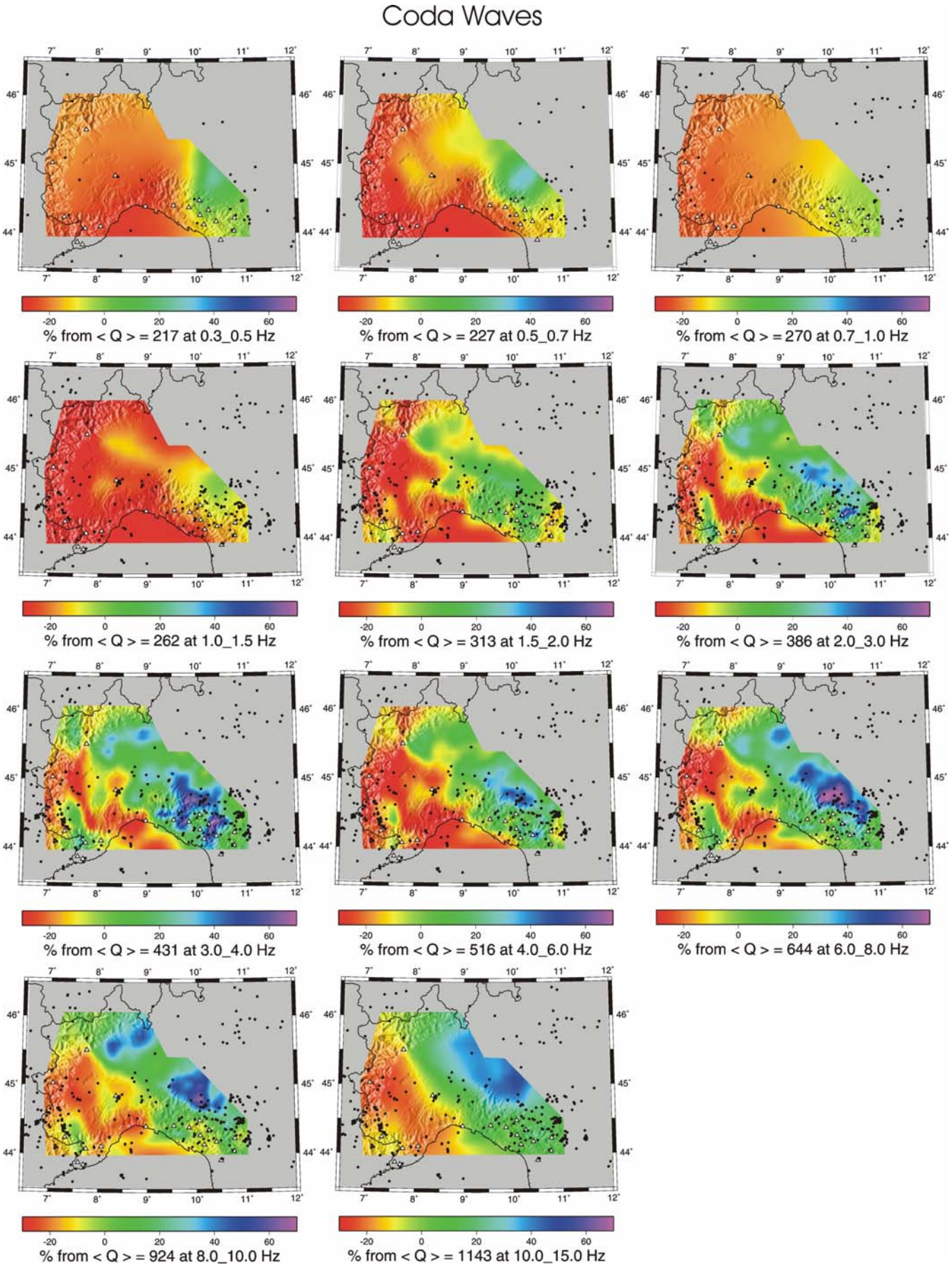

Figure 5 - Q tomography results for coda waves at all frequency bands. Each image shows the variation of Q in percentage with respect to the average value reported at the bottom of each image (<Q>). The

colored portion of each map delineated the region where we have good resolution. White triangles represent the stations while black circles are the events used for each inversion.

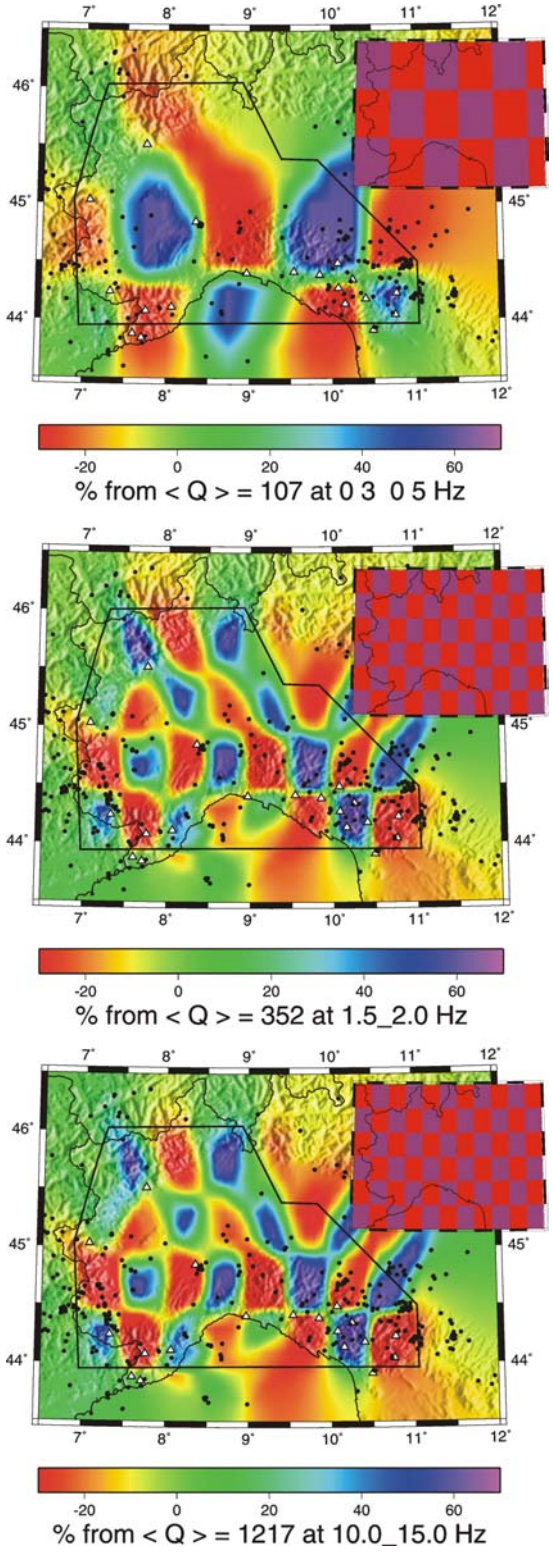

Figure 6 - Result of checkerboard tests for the frequency bands 0.3-0.5 Hz, adopting cell size of 1.0 X 1.0 degrees; 1.5-2.0 Hz and 10.0-15.0 Hz using cells of 0.50 degree by 0.50 degree. The input model is reported in the top corner of each image. The low and high attenuation input values vary as a function of frequency, in accordance to what we observe in the real data. The polygonal delineates the region where we have a good resolution.

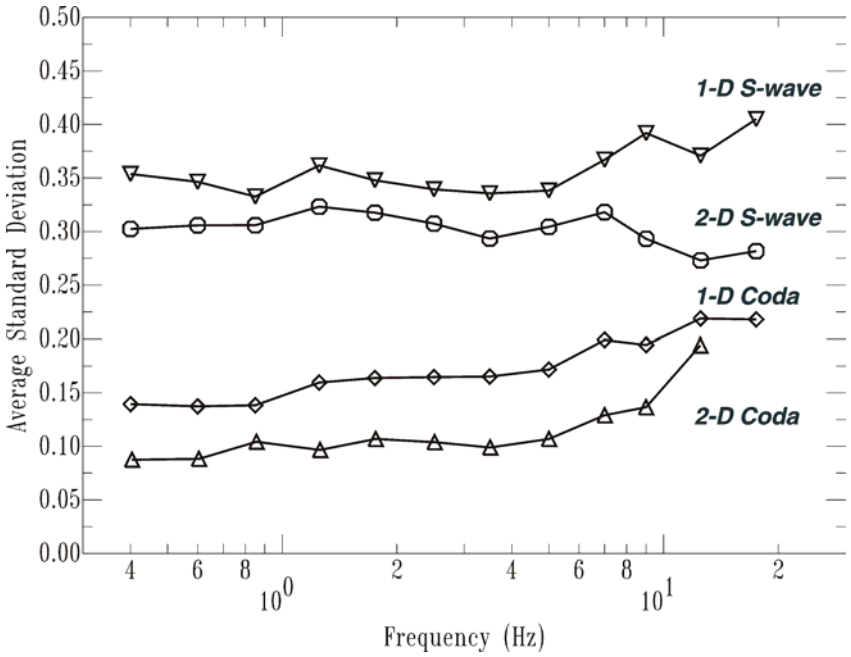

Figure 7 –Averaged inter-station standard deviation using 37 station pairs as a function of frequency. The 1-D and 2-D methodologies applied to direct and coda waves have been compared and the results show that the tomographic method (2-D) applied on coda waves gives the best results with the lowest standard deviations.

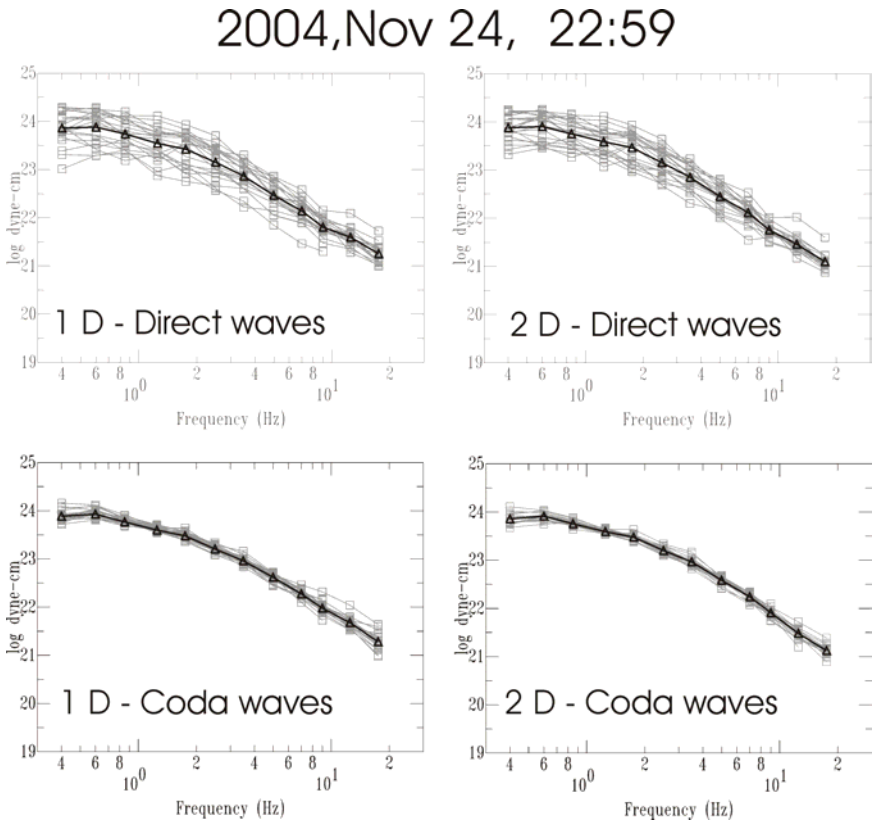

Figure 8 – Example of moment rate spectra obtained for the 2002, November 24th, M_W=5.1 event. Gray curves are the individual station spectra while black curves represent the averages. Stations are situated at a variety of azimuths and distances. The direct waves results are more scattered then coda waves for both 1-D and 2-D methods. This result is also observable in figure 7.